2007 IEEE International Conference on
Robotics and Automation
Roma, Italy, 10-14 April 2007

Stable Non-linear Force/Position Mapping for Enhanced Telemanipulation of Soft Environments

Pawel Malysz and Shahin Sirouspour
Department of Electrical and Computer Engineering, McMaster University
Hamilton, Ontario L8S 4K1, Canada
malyszp@mcmaster.ca, sirouspour@ece.mcmaster.ca

***Abstract*— The performance index in bilateral teleoperation, transparency, is often defined as linear scaling between the master and slave positions, as well as the operator and environment forces. Motivated by applications involving soft tissue manipulation such as robotic surgery, the transparency objective is generalized to include monotonic nonlinear mappings between the master/slave position and force signals. Modified Lyapunov-based adaptive motion/force controllers are presented that can guarantee the convergence of position and force tracking errors in the presence of dynamic uncertainty. Given a priori known bounds on the unknown operator and environment mass-spring-damper parameters, the closed-loop stability is analyzed using an off-axis circle criterion and the Nyquist envelope of interval plant systems. This approach produces far less conservative stability margins than those achievable by the passivity analysis. Experimental results with a two-axis teleoperation setup are provided.**

***Index Terms*— Teleoperation, Telemanipulation, Telesurgery, Robotic surgery, Soft tissue manipulation, Transparency, Circle criterion, Adaptive control**

I. INTRODUCTION

Teleoperation allows one to extend his/her manipulation skills and intelligence to different environments through coordinated control of two robotic arms. Increased interest in robotic-assisted surgery has emerged since it can grant the surgeon super-human capabilities such as increased precision and/or enhanced sensitivity through haptic feedback and force/position scaling. Among its other benefits are reduced patient trauma due to minimal invasiveness, and the possibility of performing remote surgery. The ability to reshape the surgeon's perception of the tissue in robotic surgery has spurred increased research into soft-environment teleoperation. To improve the outcome of surgical procedures, new task-specific design performance criteria are being sought that will replace the conventional transparency measures.

In soft-tissue manipulation the design objectives focus more on the fidelity of the system. Traditional measures of fidelity involved making the system transparent by matching environment and transmitted impedances, or equivalently establishing force and position tracking between the master and slave [1]. The work of Colgate in [2] is one of the early attempts at altering the operator's feel of the task through robust linear impedance shaping.

More recently, optimization of task-based fidelity measures have been proposed for soft-tissue telemanipulation [3], [4]. In these methods the fidelity measure is optimized to provide increased sensitivity to differential thresholds while maintaining stability over a range of operator and environment parameters. A drawback of these robust but nonadaptive controllers is their inherent conservatism. In [5], Wang et al. have used an optimization based method, and have added a heuristic adaptive environment impedance estimation to improve system fidelity. However, the stability of this approach is not guaranteed [5]. Moreover, all these methods ultimately result in linear scalings of position and force signals.

The use of nonlinear position and force mappings in soft-tissue manipulation can provide greater flexibility in shaping the surgeon's perception. The design of such nonlinear mappings requires comprehensive human factors studies and remains beyond the scope of the current work. Instead, the focus of this paper will be on the design of teleoperation controllers that can enforce desired monotonic nonlinear force and position scalings, and their stability analysis. Communication delay is assumed to be negligible since the surgeon and robot can be assumed to be in the same room.

The adaptive nonlinear motion/force teleoperation controllers proposed in [6] are modified to accommodate nonlinear mappings. These controller incorporate nonlinear models of the master and slave robots, as well as linear models of the operator's arm and the environment, all subject to parametric uncertainty. Nonlinear force and position mappings, and an adjustable virtual intervening tool dynamics are established between the master and slave devices. Given an expected range of hand/environment impedances to be encountered during soft-tissue telemanipulation, stability of the teleoperation system is analyzed using a combination of an off-axis circle criterion and the Nyquist envelope of interval plant control systems [7], [8]. The stability anlysis given will apply when either non-linear force *or* position mapping is used, however the proposed control architecture can accommodate *both* non-linear mappings.

In summary, the main contributions of this paper are: an adaptive master/slave four-channel teleoperation controller that handles non-linear force/position mappings, its stability analysis and experimental results on a two-axis teleoperation system. The rest of the paper is organized as follows. The dynamics of the master and slave systems are discussed in Section II. The proposed non-linear controller is presented in Section III. The stability proof and analysis are given in Section IV. Experimental results are presented in Section V. Concluding remarks are given in Section VI.

1-4244-0602-1/07/$20.00 ©2007 IEEE.

II. DYNAMICS OF MASTER/SLAVE SYSTEMS

The dynamics of the master ($\gamma = m$) and slave ($\gamma = s$) robots have the following general nonlinear form [9]:

$$D_\gamma(x_\gamma)\ddot{x}_\gamma + C_\gamma(x_\gamma, \dot{x}_\gamma)\dot{x}_\gamma + G_\gamma(x_\gamma) = F_\gamma - F_{ext,\gamma} \quad (1)$$

where x_γ is the workspace position vector, $D_\gamma(x_\gamma)$ is a positive definite mass matrix, $C_\gamma(x_\gamma, \dot{x}_\gamma)$ represents velocity dependent elements such as Coriolis and centrifugal effects, $G_\gamma(x_\gamma)$ corresponds to position-dependent forces such as gravity, F_γ is robot control force and $F_{ext,\gamma}$ represents external forces at the robot end-effector.

The external forces on the master and slave robots correspond to the hand and environment forces respectively; their relationships are shown below in (2) and (3). To simplify the design and analysis, the environment and operator dynamics are assumed to be second-order decoupled LTI models. Such models have been successfully used by other researchers [6]

$$F_{ext,s} = F_e = M_e\ddot{x}_s + B_e\dot{x}_s + K_e[x_s - x_{s0}] \quad (2)$$

$$F_{ext,m} = -F_h = \\ -(F_h^* - M_h\ddot{x}_m - B_h\dot{x}_m - K_h[x_m - x_{m0}]) \quad (3)$$

where M_e, M_h, B_e, B_h, K_e and K_h are positive diagonal matrices corresponding to mass, damping and stiffness, F_h^* is the human exogenous force subject to (4), and x_{s0} and x_{m0} represent the contact points of environment and hand.

$$\|F_h^*\|_\infty \leq \quad \alpha_h < +\infty, \qquad \alpha_h > \quad 0 \quad (4)$$

Using (1), (2) and (3), the dynamics of the master and slave systems can be represented by (5) and (6) respectively.

$$\mathcal{M}_m\ddot{x}_m + \mathcal{C}_m\dot{x}_m + \mathcal{G}_m = F_m + F_h^* \quad (5)$$
$$\mathcal{M}_m = D_m(x_m) + M_h \quad , \mathcal{C}_m = C_m(\dot{x}_m, x_m) + B_h$$
$$\mathcal{G}_m = G_m(x_m) + K_h[x_m - x_{m0}]$$

$$\mathcal{M}_s\ddot{x}_s + \mathcal{C}_s\dot{x}_s + \mathcal{G}_s = F_s \quad (6)$$
$$\mathcal{M}_s = D_s(x_s) + M_e, \quad \mathcal{C}_s = C_s(\dot{x}_s, x_s) + B_e$$
$$\mathcal{G}_s = G_s(x_s) + K_e[x_s - x_{s0}]$$

To facilitate the teleoperation control design, the slave dynamics are rewritten in mapped coordinates. By combining memoryless nonlinear monotonic mapping $\kappa_p(x_s)$ and its derivatives given in (7) with the slave dynamics in (6), the new slave dynamics can be obtained in (8).

$$q_s = \kappa_p(x_s), \quad \dot{q}_s = \dot{\kappa}_p(x_s) = J\dot{x}_s \quad (7)$$
$$\ddot{q}_s = \ddot{\kappa}_p(x_s) = J\ddot{x}_s + \dot{J}\dot{x}_s$$

$$\mathcal{M}_s'\ddot{q}_s + \mathcal{C}_s'\dot{q}_s + J^{-T}\mathcal{G}_s = J^{-T}F_s \quad (8)$$
$$\mathcal{M}_s' = J^{-T}\mathcal{M}_sJ^{-1}, \quad \mathcal{C}_s' = J^{-T}[\mathcal{C}_s - \mathcal{M}_sJ^{-1}\dot{J}]J^{-1} \quad (9)$$

where $J = \frac{\partial\kappa(.)}{\partial x_s}$ is a configuration-dependent Jacobian matrix. It can be shown that the skew-symmetry property of $\dot{\mathcal{M}}_s - 2\mathcal{C}_s$ is preserved under the above nonlinear coordinate transformation, i.e. $\dot{\mathcal{M}}_s' - 2\mathcal{C}_s'$ is also skew-symmetric, as long as J is nonsingular.

III. CONTROL DESIGN

A. Adaptive Master/Slave Controllers

The local control laws for the master and slave are given in (10) and (11), respectively.

$$F_m = \quad Y_m\hat{\Theta}_m + \mathcal{K}_m(v_{md} - v_m + A\tilde{F}_h) - \\ \alpha_h\text{sign}(v_{md} - v_m + A\tilde{F}_h) \quad (10)$$
$$F_s = \quad J^T[Y_s\hat{\Theta}_s + \mathcal{K}_s(v_{sd} - \dot{\kappa}_p(x_s) - A\kappa_f(\tilde{F}_e))] \quad (11)$$

where v_{md} and v_{sd} are master and slave command vectors to be introduced later, $\mathcal{K}_m, \mathcal{K}_s > 0$, $A > 0$ are diagonal matrices, $\tilde{F}_\gamma$ is a filtered force obtained from (12), and $\kappa_f(\cdot)$ is a monotonic nonlinear force mapping.

$$\dot{\tilde{F}}_\gamma = C(F_\gamma - \tilde{F}_\gamma) \quad (12)$$

$C > 0$ is diagonal. In (10) and (11), $\hat{\Theta}_\gamma$ denotes the estimate of Θ_γ which contains all unknown dynamic parameters of the master ($\gamma = m$) or slave ($\gamma = s$). Furthermore, Y_m and Y_s are regressor matrices defined by

$$Y_s\Theta_s = \quad \mathcal{M}_s'\tfrac{d}{dt}[v_{sd} - A\kappa_f(\tilde{F}_e)] + \\ \mathcal{C}_s'[v_{sd} - A\kappa_f(\tilde{F}_e)] + J^{-T}\mathcal{G}_s \quad (13)$$
$$Y_m\Theta_m = \quad \mathcal{M}_m\tfrac{d}{dt}[v_{md} + A\tilde{F}_h] + \\ \mathcal{C}_m[v_{md} + A\tilde{F}_h] + \mathcal{G}_m \quad (14)$$

The parameter adaptation laws are governed by

$$\dot{\hat{\Theta}}_{\gamma i} = \begin{cases} 0, & \hat{\Theta}_{\gamma i} \leq \Theta_{\gamma i}^- \text{ and } Y_{\gamma i}^T\rho_\gamma \leq 0 \\ 0, & \hat{\Theta}_{\gamma i} \geq \Theta_{\gamma i}^+ \text{ and } Y_{\gamma i}^T\rho_\gamma \geq 0 \\ \Gamma_{\gamma i}Y_{\gamma i}^T\rho_\gamma, & \text{otherwise} \end{cases} \quad (15)$$

$$\rho_s = v_{sd} - \dot{\kappa}_p(x_s) - A\kappa_f(\tilde{F}_e) \quad (16)$$
$$\rho_m = v_{md} - v_m + A\tilde{F}_h \quad (17)$$

where γi denotes the ith parameter of either master ($\gamma = m$) or slave ($\gamma = s$), $\Gamma_{\gamma i} > 0$ represents a parameter update gain, $\Theta_{\gamma i}^-$ and $\Theta_{\gamma i}^+$ denote the minimum and maximum allowable values of $\Theta_{\gamma i}$, and $\tilde{\Theta} = \hat{\Theta} - \Theta$.

Using the Lyapunov function for the master subsystem in (18), it is straightforward to show (19), where (5), (10), (14), (15), and the skew-symmetry of $\dot{\mathcal{M}}_m - 2\mathcal{C}_m$ have been employed.

$$V_m = \quad \tfrac{1}{2}\rho_m^T\mathcal{M}_m\rho_m + \tilde{\Theta}_m^T\Gamma_m\tilde{\Theta}_m \quad (18)$$

$$\dot{V}_m \leq \quad -\rho_m^T\mathcal{K}_m\rho_m \quad (19)$$

Similarly the following Lyapunov function (20) is defined for the slave subsystem. Again using (8), (11), (13), (15), and the skew-symmetry of $\dot{\mathcal{M}}_s' - 2\mathcal{C}_s'$, one may obtain (21).

$$V_s = \quad \tfrac{1}{2}\rho_s^T\mathcal{M}_s'\rho_s + \tilde{\Theta}_s^T\Gamma_s\tilde{\Theta}_s \quad (20)$$

$$\dot{V}_s \leq \quad -\rho_s^T\mathcal{K}_s\rho_s \quad (21)$$

Finally, using (18), (20), (19), and (21), it can be concluded

$$\rho_s \in L_2 \cap L_\infty, \qquad \rho_m \in L_2 \cap L_\infty \quad (22)$$

B. Teleoperation

For bilateral teleoperation with non-linear force/position mappings the command vectors are designed as follows:

$$v_{sd} = \tilde{v}_m + \Lambda[\tilde{x}_m - \kappa_p(x_s)] + A\tilde{F}_h \quad (23)$$

$$v_{md} = \dot{\tilde{\kappa}}_p(x_s) + \Lambda[\tilde{\kappa}_p(x_s) - x_m] - A\kappa_f(\tilde{F}_e) \quad (24)$$

where $\Lambda > 0$ is diagonal. Let $Q = x_m, v_m, \kappa_p(x_s), \dot{\kappa}_p(x_s)$, then $\tilde{Q}$ can be computed from the following filter

$$\dot{\tilde{Q}} + C\tilde{Q} = CQ \quad (25)$$

Substituting (23) and (24) into (16) and (17), and performing addition and substraction yield

$$\rho_s - \rho_m = \tilde{v}_m - \dot{\tilde{\kappa}}_p(x_s) + \Lambda[\tilde{x}_m - \tilde{\kappa}_p(x_s)] + v_m - \dot{\kappa}_p(x_s) + \Lambda[x_m - \kappa_p(x_s)] \quad (26)$$

$$\rho_s + \rho_m = -C^{-1}[\dot{\tilde{v}}_m + \ddot{\tilde{\kappa}}_p(x_s) + \Lambda\dot{\tilde{x}}_m + \Lambda\dot{\tilde{\kappa}}_p(x_s)] + 2A[\tilde{F}_h - \kappa_f(\tilde{F}_e)] \quad (27)$$

Using Lemma 1 from [6] and (26) it follows that

$$\rho_e = x_m - \kappa_p(x_s) \in L_2 \cap L_\infty \quad (28)$$

$$\rho_p = v_m - \dot{\kappa}_p(x_s) \in L_2 \cap L_\infty \quad (29)$$

This guarantees L_2 and L_∞ stability for both position and velocity tracking errors. Using (28) and (29), Eq. (27) can be rewritten as:

$$\tilde{F}_h - \kappa_f(\tilde{F}_e) - \bar{\rho} = (AC)^{-1}(s + \Lambda)\tilde{v}_m = \mathcal{Z}_t\tilde{x}_m \quad (30)$$

where

$$\bar{\rho} = \frac{1}{2A}[\rho_s + \rho_m - C^{-1}(s + \Lambda)\tilde{\rho}_p] \in L_2 \cap L_\infty \quad (31)$$

and $\mathcal{Z}_t$ is a virtual tool impedance with mass specified by $(AC)^{-1}$ and damping specified by $\Lambda(AC)^{-1}$.

The adaptive controllers decouple the closed-loop dynamics in different axes of motion. Therefore throughout the rest of the paper, without loss of generality, only one axis is considered. Using the LTI models of the hand and environment (32), the transparency equation (30) and position tracking error in (28), the teleoperation system can be reduced to the block diagram shown in Fig. 1(a).

$$F_e = \mathcal{Z}_e x_s, \quad F_h = F_h^* - \mathcal{Z}_h x_m \quad (32)$$

Assuming both mappings are linear leads to the guaranteed stability result obtained in [6], i.e.

$$\rho_m, \rho_s, \rho_e, \rho_p, \bar{\rho} \to 0 \quad (33)$$

$$v_m, v_s \in L_\infty \quad (34)$$

In the more general case of nonlinear position and force mapping, new conditions for robust stability must be derived as will be discussed in the next section. It should be noted that Eqs. (28) and (29) demonstrate nonlinear position/velocity tracking between master and slave. Also according to (30), the operator would feel the mapped environment force through an intervening tool with adjustable mass and damping parameters. Under quasi-static conditions, the user's hand force and mapped environment force would track each other.

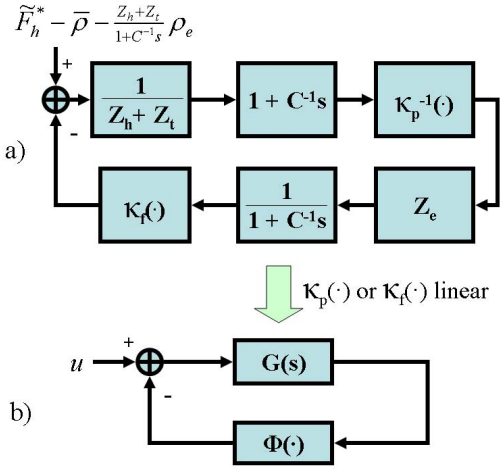

Fig. 1. Teleoperation block diagram: (a) original (b) transformed to the classic Lur'e form when $\kappa_p()$ or $\kappa_f()$ is linear.

IV. NON-LINEAR FEEDBACK STABILITY

As shown in Fig. 1, it is possible to convert the teleoperation block diagram to a non-linear Lur'e type problem [10] by assuming that one of the two mappings is linear, i.e. by considering the linear position/nonlinear force or nonlinear position/linear force mapping combinations. In such a case, the linear part would reduce to (35) with non-linear feedback element (36) and an exogenous input defined in (37).

$$G(s) = \frac{m_1 s^2 + b_1 s + k_1}{m_2 s^2 + b_2 s + k_2} = \frac{\mathcal{Z}_e}{\mathcal{Z}_h + \mathcal{Z}_t} \quad (35)$$

$$\Phi(\cdot) = \begin{cases} \kappa_f(\cdot)\kappa_p^{-1} & \kappa_p(\cdot) \text{ linear} \\ \kappa_p^{-1}(\cdot)\kappa_f & \kappa_f(\cdot) \text{ linear} \end{cases} \quad (36)$$

$$u = \begin{cases} \tilde{F}_h^* - \bar{\rho} - \frac{\mathcal{Z}_h+\mathcal{Z}_t}{1+C^{-1}s}\rho_e & \kappa_p(\cdot) \text{ linear} \\ -\frac{F_h^*}{\kappa_f \mathcal{Z}_e} + \frac{1+C^{-1}s}{\kappa_f \mathcal{Z}_e}\bar{\rho} + \frac{\mathcal{Z}_h+\mathcal{Z}_t}{\kappa_f \mathcal{Z}_e}\rho_e & \kappa_f(\cdot) \text{ linear} \end{cases} \quad (37)$$

where $m_1 \geq 0$, $b_1 \geq 0$, $k_1 \geq 0$ represent environment impedance parameters and $m_2 = m_h + m_t > 0$, $b_2 = b_h + b_t > 0$, $k_2 \geq 0$ represent the combined impedance parameters of the hand and virtual tool.

For nonlinear elements belonging to the first and third quadrants, i.e. $x\Phi(x) \geq 0$, a sufficient condition for the stability of the feedback system in 1(b) is strict positive realness (SPR) of the linear element [10], i.e.

$$\inf_{\omega \in \Re} \text{Re}\left(\frac{-m_1\omega^2 + b_1 j\omega + k_1}{-m_2\omega^2 + b_2 j\omega + k_2}\right) > 0 \quad (38)$$

The condition in (38) can be shown to be equivalent to:

$$b_1 b_2 > \left(\sqrt{m_1 k_2} - \sqrt{m_2 k_1}\right)^2 \quad (39)$$

which must be satisfied for all possible combinations of hand and environment parameters. In practice, allowing all possible environment and hand impedances results in large perturbations in $G(s)$ making stability, if possible, challenging to guarantee. However, it is reasonable to assume that the parameters have limits that depend on application. In Table I, a hypothetical example of such bounds for soft-tissue manipulation is given. Using (39), (35) with a desired

tool mass of $m_t = 0.4$ kg, and the data in Table I, the minimum level of virtual tool damping needed for $G(s)$ to be SPR is $b_t > 135\ Nsm^{-1}$. Assuming negligible tool mass, $m_t \approx 0$, yields $b_t > 57\ Nsm^{-1}$. Clearly these levels of damping are too high to provide good fidelity for soft-tissue telemanipulation and therefore, alternative stability conditions must be considered.

An off-axis circle criterion can produce a far less conservative sufficient stability condition at the expense of more restriction on the nonlinear element. Assume that Φ belongs to an incremental sector $[a, b]$, i.e.

$$\begin{aligned} &(i) \quad \Phi(0) = 0 \\ &(ii) \quad a \leq \frac{\Phi(x_1) - \Phi(x_2)}{x_1 - x_2} \leq b \end{aligned} \tag{40}$$

Then the feedback loop in Fig. 1(b) is stable if the Nyquist plot of G(s) lies outside a circle which intersects $-\frac{1}{a}$ and $-\frac{1}{b}$ on the real axis [7] (see Fig. 2). Using the transformation given in (41), this requirement can be restated as (42).

$$\begin{aligned} H(s) &= \frac{G(s) + \frac{1}{2}(\frac{1}{a} + \frac{1}{b}) - dj - r}{G(s) + \frac{1}{2}(\frac{1}{a} + \frac{1}{b}) - dj + r} \\ r &= \sqrt{d^2 + \frac{1}{4}\left(\frac{1}{a} - \frac{1}{b}\right)^2}, d \in \Re \end{aligned} \tag{41}$$

$$\inf_{\omega \in \Re^+} \mathrm{Re}\left(H(j\omega)\right) > 0 \tag{42}$$

The condition in (42) states that the Nyquist plot of $G(s)$ does not enter a circle whose centre has imaginary component equal to d and intersects the real axis at $-\frac{1}{a}$ and $-\frac{1}{b}$, if and only if the real part of $H(j\omega)$ is positive for $\forall \omega \in \Re^+$. For $d = 0$ (42) reduces to the on-axis circle criterion which does not require monotonicity of $\Phi(\cdot)$ [10], but is more conservative (see Fig. 2).

It should be noted that $G(s)$ is not a single transfer function but rather a family of transfer functions with independent real interval coefficients; thus $G(s)$ represents an interval plant system [8]. When dealing with interval plant systems with independent coefficients one typically is interested in Kharitonov polynomials. For a polynomial function $\mathcal{F}(s) = \delta_0 + \delta_1 s + \delta_2 s^2 + ...$, $\delta_i^- \leq \delta_i \leq \delta_i^+$, with real interval coefficients four Kharitonov polynomials are defined as follows [11]:

$$\begin{aligned} \mathcal{K}_{\mathcal{F}}^1(s) &= \mathcal{K}_{\mathcal{F}}^{even,min}(s) + \mathcal{K}_{\mathcal{F}}^{odd,min}(s) \\ &= \delta_0^- + \delta_1^- s + \delta_2^+ s^2 + \delta_3^+ s^3 + ... \\ \mathcal{K}_{\mathcal{F}}^2(s) &= \mathcal{K}_{\mathcal{F}}^{even,min}(s) + \mathcal{K}_{\mathcal{F}}^{odd,max}(s) \\ &= \delta_0^- + \delta_1^+ s + \delta_2^+ s^2 + \delta_3^- s^3 + ... \\ \mathcal{K}_{\mathcal{F}}^3(s) &= \mathcal{K}_{\mathcal{F}}^{even,max}(s) + \mathcal{K}_{\mathcal{F}}^{odd,min}(s) \\ &= \delta_0^+ + \delta_1^- s + \delta_2^- s^2 + \delta_3^+ s^3 + ... \\ \mathcal{K}_{\mathcal{F}}^4(s) &= \mathcal{K}_{\mathcal{F}}^{even,max}(s) + \mathcal{K}_{\mathcal{F}}^{odd,max}(s) \\ &= \delta_0^+ + \delta_1^+ s + \delta_2^- s^2 + \delta_3^- s^3 + ... \end{aligned} \tag{43}$$

For a transfer function $T(s) = \frac{\mathcal{N}(s)}{\mathcal{D}(s)}$ with independent interval coefficients in the numerator and denominator, 16 Kharitonov plants can be defined as follows

$$T_K(s) = \left\{ \frac{\mathcal{K}_{\mathcal{N}}^i}{\mathcal{K}_{\mathcal{D}}^j} : i, j \in \{1, 2, 3, 4\} \right\} \tag{44}$$

$H(s)$ is also an interval plant system whose coefficients may be complex and depend linearly on the coefficients of $G(s)$. To determine if (42) is satisfied for the interval system $H(s)$, it is sufficient to check if (42) is satisfied for the 16 Kharitonov plants $G_K(s)$. The proof of this lies in the fact that for $\omega \in \Re^+$ the outer Nyquist envelope of the interval system $G(s)$ can be found from the union of the Nyquist plots of $G_K(s)$ [8]. Therefore if the Nyquist envelope of $G(s)$ lies outside the circle specified by a, b and d, then $Re(H(j\omega)) > 0$ for $\forall \omega \in \Re^+$. The benefit of using (42) is that it is no longer a graphical test as is shown in Fig 2.

Given a, an upper value of b, $b \geq a$, can be found by searching through the two dimensional space of $b \in \Re^+$ and $d \in \Re$ using (42) as a stability constraint. This has been done using both the on-axis and off-axis circle criterions with the intervals specified in Table I. Fig. 3 shows the results of such an analysis with virtual tool parameters of $m_t = 0.4$ kg and $b_t = 10\ Nsm^{-1}$. Among the design parameters, the virtual tool damping has the biggest impact on the closed-loop stability. This can be observed in Fig. 4 where the stability margins derived from the off-axis circle criterion have increased at the expense of higher tool damping.

Finally, it should be noted that in Fig. 1(b), $u \in L_\infty$ since $F_h^* \in L_\infty$. Although the sufficient conditions in this section have been originally developed for L_2 stability, they can be generalized to L_∞ stability [12], [10] and hence are applicable to the problem studied here.

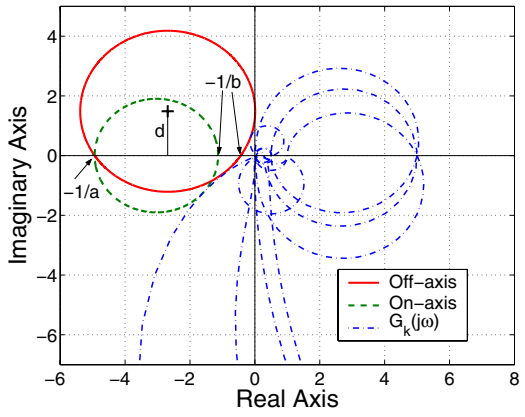

Fig. 2. The off-axis vs. on-axis circle criterion test for a family of transfer functions; given a lower sector bound a, the off-axis criterion results in a larger upper sector bound b.

TABLE I

PARAMETER RANGES FOR HAND AND ENVIRONMENT

	Mass (kg)	Damping (Nsm^{-1})	Stiffness (Nm^{-1})
$\mathcal{Z}_e$	0.01–0.2	5–50	10-1000
$\mathcal{Z}_h$	0-0.3	0–100	20-1000

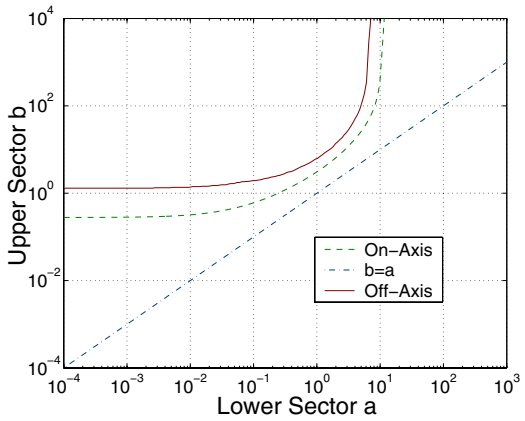

Fig. 3. Off-axis vs. on-axis circle criterion: the stable region is between the straight and curved lines.

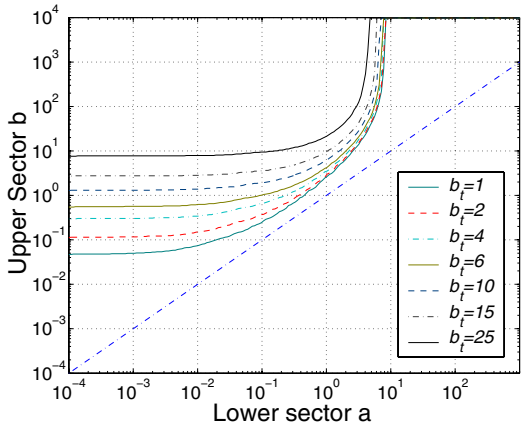

Fig. 4. Stability regions obtained from the off-axis circle criterion for different values of virtual tool damping b_t.

V. EXPERIMENTAL RESULTS

A master/slave experimental platform shown in Fig. 5 has been used to evaluate the proposed teleoperation controller. Two Quanser pantograph mechanisms each with two active axes of motion in the x-y plane have been employed as master and slave robots. The pantograph devices are actuated by two direct-drive DC motors attached to the proximal links. The motor shaft angles are measured by optical encoders with $20,000$ counts per revolution. Two Mini40 force/torque sensors from ATI Industrial Automation have been attached to the mechanisms end-effectors to measure the hand and environment interaction forces. Sponge is used to create the effect of a soft tissue. The control code runs under Matlab RTW/Torndao VxWorks real-time operating system with a sampling frequency of 2048 Hz.

The pantograph devices are light, have low-friction and are easily backdrivable. The mass of the force sensor and end-effector attachments dominate the device dynamics, justifying the use of linear decoupled mass-spring-models in the workspace coordinates for the control design. Position-dependent variations in the device dynamics due to non-linearities can be adapted for by the local master/slave controllers. To deal with the human exogenous force F_h^*, the control law in (10) employs a switching element that

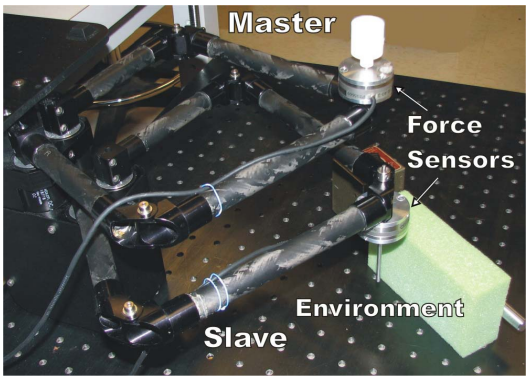

Fig. 5. The two-axis experimental setup.

can cause unwanted chattering in the control signal. For the experiment the master controller was modified such that it would adapt for F_h^* by adding it to the feedforward term (14). This is acceptable provided the adaptation is much faster than the rate of change in F_h^*. The controller parameters used in the experiment trials are given in Table II.

A. Nonlinear force mapping

The first experiment was conducted using a linear position mapping of $\kappa_p(x) = 2x$ and a nonlinear monotonic force mapping of $\kappa_f(f) = 2\tanh(2f) + 0.25f$ which result in $\kappa_p()^{-1}\kappa_f() \in [0.125, 2.125]$. During the experiment, the operator moved the master device in free motion and made several stable contacts with the environment. The teleoperation controller rapidly adapted to the environment stiffness variations and produced accurate mappings between the master/slave position and force signals, as shown in Fig. 6(a),(b). The resulting force mappings in the $(f_h - f_e)$ planes for the x and y coordinates are compared with the desired force mapping in Fig. 6(c), from which it is clear that the design objective has been achieved. It should be pointed out that the force changes during the contact have been deliberately performed by the operator to demonstrate the force tracking. Also the non-zero operator force in free motion is due to the intervening tool dynamics.

B. Nonlinear position mapping

The second experiment was conducted using a nonlinear monotonic position mapping of $\kappa_p(x) = 1.5x\tanh^2(6x) + 0.5x$ and a linear force mapping of $\kappa_f(f) = f$ which result in $\kappa_p()^{-1}\kappa_f() \in [0.4, 2]$. As in the previous case, the operator performed free motion maneuver and made several stable contacts with the environment. The position and force tracking objectives have been satisfied, as seen in Figs. 6(d), (e) and (f).

TABLE II
CONTROLLER PARAMETERS

A	C	Λ	$\mathcal{K}_s, \mathcal{K}_m$	Γ_s,Γ_m
0.02 $kg^{-1}s$	40π rad/s	10 s^{-1}	35 Nsm^{-1}	1000-25000000

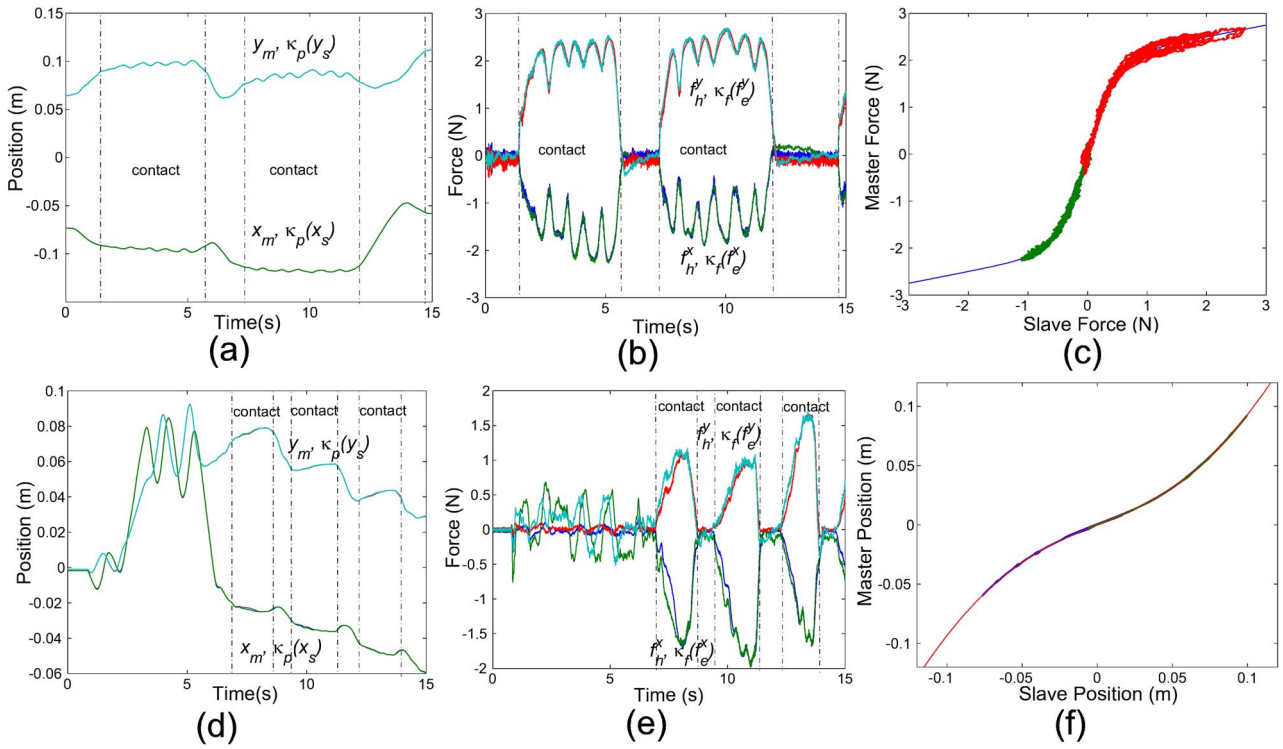

Fig. 6. Experimental results: nonlinear force mapping (a) position tracking (b) force tracking (c) force mapping; nonlinear position mapping (d) position tracking (e) force tracking (f) position mapping. Note the position tracking graphs a) and d) actually contain four signals.

VI. CONCLUSIONS AND FUTURE WORK

A growing interest in robotic-assisted surgical applications has prompted researchers to explore new teleoperation control methods for enhancing the fidelity of haptic interaction with soft tissues. While previous relevant research has mainly focused on linear scalings of the positions, forces and impedances, in this paper, nonlinear mappings of positions and forces were proposed. It is anticipated that the greater flexility offered by such mappings can lead to the design of enhanced teleoperation controllers for soft-tissue telemanipulation.

As the first step towards the above-stated goal, a modified adaptive motion/force teleoperation controller was proposed that can establish desired monotonic nonlinear mappings between the master and slave in the presence of dynamic parametric uncertainties. Using a combination of an off-axis circle criterion for static monotonic nonlinearities and the Nyquist envelop of interval plants, sufficient regions of stability were obtained for a given range of hand/environment parameters which are far less restrictive than those obtained from the passivity and on-axis circle theorems. The proposed method was validated in experiments with a 2DOF master/slave system.

Future research will involve human factors experiments to determine the types of nonlinearities that can enhance the sensitivity/performance of soft-tissue manipulation.

ACKNOWLEDGMENTS

The authors gratefully acknowledge the Natural Sciences and Engineering Research Council of Canada (NSERC) and MDA Space Missions for supporting this project, and WindRiver Corp. for the donation of Tornado/vxWorks RTOS.

REFERENCES

[1] D. Lawrence, "Stability and transparency in bilateral teleoperation," *IEEE Trans. Robot. Automat.*, vol. 9, pp. 624–637, October 1993.

[2] J. Colgate, "Robust impedance shaping telemanipulation," *IEEE Trans. Robot. Automat.*, vol. 9, pp. 374–384, August 1993.

[3] M. Çavuşoğlu, A. Sherman, and F. Tendick, "Design of bilateral teleoperation controllers for haptic exploration and telemanipulation of soft environments," *IEEE Trans. Robot. Automat.*, vol. 18, no. 4, pp. 641–647, 2002.

[4] G. D. Gersem, H. V. Brussel, and F. Tendick, "Reliable and enhanced stiffness perception in soft-tissue telemanipulation," *Int. J. Robot. Research*, vol. 24, no. 10, pp. 805–822, 2005.

[5] X. Wang, P. X. Liu, B. Chebbi, D. Wang, and M. Meng, "Design of bilateral teleoperators for soft environments with adaptive environmental impedance estimation," in *Proc. IEEE Int. Conf. Robotics Automation*, pp. 1127–1132, 2005.

[6] W. Zhu and S. Salcudean, "Stability guaranteed teleoperation: an adaptive motion/force control approach," *IEEE Trans. Automat. Contr.*, vol. 45, pp. 1951–1969, November 2000.

[7] Y.-S. Cho and K. S. Narendra, "An off-axis circle criterion for the stability of feedback systems with a monotonic nonlinearity," *IEEE Tran. Automat. Cont.*, vol. 13, no. 4, pp. 413–416, 1968.

[8] C. V. Hollot and R. Temp, "On the nyquist envelope of an interval plant family," *IEEE Tran. Automat. Cont.*, vol. 39, no. 2, pp. 391–396, 1994.

[9] L. Sciavicco and B. Siciliano, *Modeling and Control of Robot Manipulators, Second Edition*. Springer-Verlag, 2000.

[10] M. Vidyasagar, *Nonlinear Systems Analysis*. Englewood Cliffs NJ: Prentice Hall, 1993.

[11] V. L. Kharitonov, "Asymptotic stability of an equilibrium position of a family of systems of linear differential equations," *Differential Equations*, vol. 14, pp. 1483–1485, 1979.

[12] G. Zames, "On the input-output stability of time-varying nonlinear feedback systems-part ii: conditions involving circles in the frequency plane and sector nonlinearites," *IEEE Trans. Automatic Control*, no. 8, pp. 465–476, 1966.